5-2003

Computer Simulation and Homogenization in Heating Design Optimization

Daniel K. Balls
Utah State University

COMPUTER SIMULATION AND HOMOGENIZATION IN HEATING DESIGN OPTIMIZATION

by

Daniel K. Balls

A report submitted in partial fulfillment
of the requirements for the degree

of

MASTER OF SCIENCE

in

Mathematics

UTAH STATE UNIVERSITY
Logan, Utah

2003

ABSTRACT

Computer Simulation and Homogenization

in Optimization of Heating Design

by

Daniel K. Balls, Master of Science

Utah State University, 2003

Major Professor: Dr. James Powell
Department: Mathematics and Statistics

The ability to ensure uniformity of temperature within a given finite physical region is an essential element in the success of many scientific processes, especially those that involve extreme fluctuation in temperature. Such a process is performed in an instrument called the *LightTyper* developed by Idaho Technology, Inc. of Salt Lake City Utah. This paper details the development and results of a scheme intended to obtain a heating design that ensures a high degree of temperature uniformity within the Idaho Technology instrument. Due to the experiments performed during this project, we were able to answer many questions that concerned finding an optimal design for a two-dimensional cross-section of the *LightTyper*.

(34 pages)

DEDICATION

First and foremost, I would like to dedicate the work of this project to my wonderful wife Star, whose support and inspiration I simply could not have done without.

I also want to give thanks to my children, Rachel and Caleb, for adding delight to my days and happiness to my soul.

I wish to express gratitude to my father and mother who have done an excellent work in rearing me and my siblings.

Finally I acknowledge and express gratitude for the much-needed help and strength the Father of All Creation granted me in overcoming several trials and challenges that blocked the way to my completing this work.

ACKNOWLEDGMENTS

I would like to acknowledge the help and support of several individuals who helped to make this project successful.

I wish to acknowledge the guidance and support of each member of my committee. I owe a huge debt of gratitude to my advisor Dr. James Powell whose patience, encouragement and time were indispensable. I would like to thank Dr. Joe Koebbe who provided the use of his *JHomogenizer* program which was vital to the completion of the project and has been instrumental in polishing this paper. I acknowledge Dr. Emily Stone for her support and time throughout the project and examination.

Further, I give thanks to Jeff Leek whose helpful insight and keen programming skills helped an several occasions along the way. Finally,I wish to express my thanks to Dr. David Eyre of Idaho Technology, Inc. for his role in the support process of this project. Daniel K. Balls

CONTENTS

LIST OF FIGURES

CHAPTER 1
INTRODUCTION

Idaho Technology (IT) has designed a system whereby an entire 16 x 24 grid of wells containing DNA can simultaneously be tested and analyzed for the presence of specific genetic sequences using melting curve analysis. After samples of DNA are amplified through the process of polymerase chain reaction, the vessel containing them is heated linearly with time. A key to the success of the analysis is ensuring each of the samples in the grid is at the same temperature at the same time during the process. [4]

The samples to be quantified and identified are arrayed in depressions in a preformed plastic sample tray that fits over a heating block made of aluminum. The block is positioned on top of a small circuit card on which is inscribed a heating element. Heat diffuses upward through the aluminum block and plastic tray into each sample. Unfortunately, uniformity of heating cannot be guaranteed due to the finite extent of the sample tray and consequent temperature losses through the tray edges. With the intent of obtaining a design for the circuit card that optimizes temperature uniformity in the wells, a computer model was created that simulates the flow of heat through a two-dimensional cross-section of the IT instrument. The model provides a numerical approximation to the solution of the heat equation $U_t = \nabla \cdot (D(x,y)\nabla U)$ with appropriate boundary and initial conditions. The function $U(x,y,t)$ represents the temperature at a specific two-dimensional location, (x,y), on the cross-section at a given time t, and $D(x,y)$ is the thermal diffusivity of the material at that coordinate. In addition to the instrument itself, the model simulates the flow of temperature in the air surrounding the instrument.

The model was created to serve as a means for feasibly testing a large number of designs in a relatively short period of time, thereby providing means for the identification of an optimal circuit card design. However, due to the extreme variation in diffusivity among the materials of the cross-section and consequent ultra-fine discretization that a faithful approximation necessitated, the running time of a single simulation was undesirably lengthy. Therefore, it was beneficial to apply the method of homogenization, an averaging technique,

to the problem to reduce the computational complexity.

The homogenization method is applicable to problems with functions containing inherent complex substructures. The process seeks to replace these functions with faithful averages which do not include the undesired structure. The disadvantage of using an averaged value is the result is only an approximation to the real solution. After an appropriate average is determined, the model's running time decreases significantly, making numerous simulations more practical. [1]

The optimization problem we desired to solve involved finding a heating source that, when used as the forcing function in the simulator, provided a high degree of temperature uniformity among the wells as time progresses. Given an arbitrary heat source design, we can simulate the temperatures within the wells of the *LightTyper*. Once these temperatures are known, we can test the uniformity of temperatures at corresponding locations.

We began by assuming that the heat source of the instrument was a continuous function of the form $\phi(x) = a_1 + a_2|x - \alpha|^{a_3}$, where a_1, a_2, a_3 are real numbers and α is the horizontal center of the instrument. Next we normalized ϕ so that it defined a probability density function (pdf) over the interval representing the instrument cross-section, $[0, 2\alpha]$. The purpose of the normalization was to provide a means for translating the optimal heating source, a continuous function, into a discrete design of elements on the heating circuit card. The details of this process are explained in greater detail later in the paper.

As an aside, we note that since the forcing function is a pdf and must therefore integrate to one over a relatively large interval, the function values of the profile were not large enough to produce a heating source required to obtain a proper simulation. However, inasmuch as the source output responds linearly, multiplication of the forcing function by a constant can regenerate any desired temperature.

As alluded to previously, the optimization process involved evaluating many different forcing functions. Simulations were performed using the function determined by specific choices of a_1, a_2 and a_3 as the heating source. Next, the mean of the temperatures at the center of each well was computed at 32 different time intervals, ranging from 0 to 40 seconds.

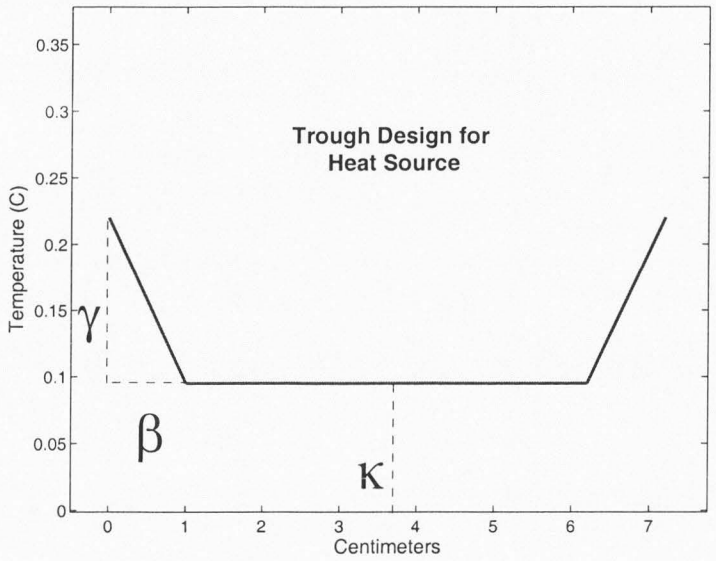

Figure 1.1. Plot of the trough design profile. This profile was used as the forcing function along $y = 0$ and given a measure according to the degree of univormity of temperature in the sample wells during the simulation that it was used. After varying β, γ and κ, and testing numerous profiles, the one with the best measure would be easily identifiable.

The temperature at the center of each well was compared with the mean temperature using various norms. The optimization process entailed varying the parameters a_1, a_2 and a_3 within an appropriate constraint range, thus producing different source functions. The function producing the greatest degree of temperature uniformity among the wells would then be deemed the optimal heating source.

The results of this initial attempt at optimization were educational. After checking literally thousands of different initial profiles, the program surprisingly deemed a *constant function* as the optimal heat source. Possible reasons for this will be presented later in the paper.

Using the knowledge of the first attempt, a second family (called *trough functions* in this paper) of profiles was constructed and examined. These profiles are piece-wise continuous functions of the form

$$\phi_2(x) = \begin{cases} -\frac{\gamma}{\beta}x + \gamma + \kappa & 0 \leq x \leq \beta \\ \kappa & \beta < x \leq \alpha \end{cases},$$

reflected around $x = \alpha$, with $\gamma > 0$ and $0 < \beta < \alpha$ (see Figure 1.1). For reasons similar

to those previously explained, the trough functions were normalized and assumed to be density functions.

The search to obtain the optimal profile among this group was conducted in a manner analogous to the previous approach. Values of β, γ, and κ were chosen and the profile they determined was used as the heating source of the simulation. This profile is given a measure according to the uniformity of temperature among the wells. As the parameters β, γ, and κ varied within their constraint ranges, a number of profiles were measured and the profile with the most desirable measure could be easily detected.

This search suggested that the optimal profile of the family is the one having parameter values $\beta = 0.4774$, $\gamma = 0.0055$, and $\kappa = 0.1385$. Though this result was arguably more informative than the previous one, the optimal profile turned out to produce a distribution function that was almost linear. This was not surprising since the bulk of the profile is a constant, and the slope of the lines on each end is minimal.

Initially, we presumed that significant adjustments needed to be made to the design of the circuit card to account for the disparate temperatures in the outer wells caused by the difficulty of heat diffusing through the plastic that surrounded them. As a consequence a number of different forcing functions, symmetric on a finite interval with higher values at the endpoints of the interval, were tested and measured for their ability to maintain consistency of temperature within the wells of the *LightTyper*. A surprising and informative result that came from the experiments described in this paper is that the edge effects do not play as significant a role as was previously thought.

As Figure 2.10 conveys, a constant forcing function is not optimal, either, as it leaves the temperature in the end wells considerably lower than that of their counterparts in the middle. Thus, in the two-dimensional cross-section, in order to obtain the optimal forcing function, one must find the proper balance between constancy within the middle wells and slight adjustment on the edges. Though the experiments conducted in this project were not able to clearly describe that balance, the method used and mistakes made should serve as a solid foundation in not only determining an optimal two-dimensional forcing function, but

eventually an optimal circuit card design.

CHAPTER 2
DETAILS OF THE PROJECT

2.1 The Analytic Problem

The mathematical model that the simulation is founded upon is a variation of the simple heat equation $U_t = D(U_{xx} + U_{yy})$, where the diffusion D is a constant. Due to the fact the the diffusion in our problem is spatially dependent, we seek an approximation to the solution U of the equation

$$U_t(x, y, t) = \nabla \cdot (D(x, y)\nabla U(x, y, t)). \qquad (2.1)$$

We note now that the the tensor $D(x, y)$ has the form $D(x, y) = \begin{pmatrix} d_{xx}(x, y) & 0 \\ 0 & d_{yy}(x, y) \end{pmatrix}$. Further, although it is the case that $d_{xx} = d_{yy}$ in the heterogenous tensor D, we will continue to distinguish the two in notation because $\overline{d}_{xx} \neq \overline{d}_{yy}$ in the homogenized tensor $\overline{D}$.

The domain of the first spatial variable, x, depends on which cross-section is being examined. For the experiments in this project, x ranges from 0 to 11.3 cm. The first two centimeters represent air, and the next 7.2 cm correspond to the machine comprised of 16 wells measuring 0.45 cm each. On the other side of the machine is an additional two centimeters of air. The final 1 cm comes from the thickness of the plastic, 0.5 cm on each side, that surrounds the outer wells. Thus in our situation, 2α represents the middle 7.3 centimeters. The second spatial variable, y, ranges from 0 to 3 cm. The line $y = 0$ represents where the circuit card meets the aluminum base of the instrument. From that point to the top of each well measures 1.6 cm, and the final 1.4 cm represents the air above the instrument. The time variable t usually ranges from 0 to 40 seconds, as it was ascertained that 40 seconds was ample time for achieving a steady thermal state.

Several assumptions provided the necessary boundary and initial conditions. First, at the beginning of the melting curve process, the entire state is assumed to be the temperature of the ambient environment, 25°. Due to the insulating nature of the circuit card materials, we require that there is no heat transfer across the line $y = 0$, which translates into the boundary condition $\frac{\partial}{\partial y}(U(x, 0, t)) = 0$. Further, certain cells along $y = 0$ are cho-

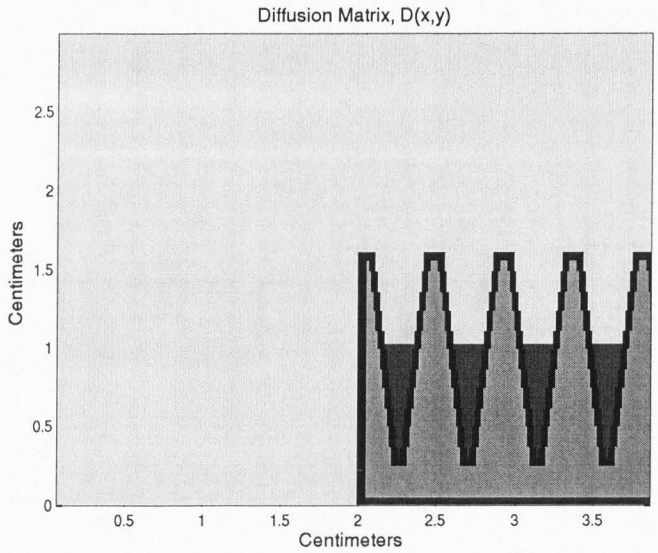

Figure 2.1. Plot of the left portion of the diffusion matrix. Dark red colors indicate high diffusivity (close to 1 $cm \cdot sec^{-2}$) while dark blue represent low diffusivity (close to 0 $cm \cdot sec^{-2}$).

sen to remain at a constant temperature of 70° and provide a forcing function along the $y = 0$ boundary. These cells represent the heating elements with a different choice of cell location constituting a different circuit design. On each side of the machine, we assume that the temperature of the air will eventually reach the ambient temperature, as will the temperature of the air above the machine. Figure 2.1 provides a graphical representation of the diffusion tensor $D(x, y)$.

2.2 The Approximation

We begin discretizing the spatial and time domains by letting $x_i = i\Delta x$, $y_j = j\Delta y$, and $t_k = k\Delta t$, where $\Delta x = \frac{4+2\alpha}{n_x}$, $\Delta y = \frac{3}{n_y}$, and $\Delta t = \frac{40}{n_t}$. In the previous definitions, n_x, n_y, and n_t represent the number of partitions in the x, y, and t domains, respectively. Thus, the physical domain of the approximation is made up from a mesh grid of the domains of x and y partitioned evenly into n_x and n_y discrete points, respectively.

If U is a solution to equation (2.1), we'll define our approximation $\widehat{U}$ by $\widehat{U}^k_{i,j} = U(x_i, y_j, t_k)$. In order to approximate the time derivatives, we'll use the standard Taylor approximation $U_t \approx \frac{1}{\Delta t}(\widehat{U}^{k+1}_{i,j} - \widehat{U}^k_{i,j}) = \Delta_t(\widehat{U})$. Similarly, spatial derivative approximations have the form

$U_x \approx \frac{1}{\Delta x}(\widehat{U}^k_{i+1,j} - \widehat{U}^k_{i,j}) = \Delta_x(\widehat{U})$ and $U_y \approx \frac{1}{\Delta y}(\widehat{U}^k_{i,j+1} - \widehat{U}^k_{i,j}) = \Delta_y(\widehat{U})$. Thus the approximation to equation (2.1) is

$$\Delta_t(\widehat{U}) = (\Delta_x, \Delta_y) \cdot \left(\begin{pmatrix} d_{xx} & 0 \\ 0 & d_{yy} \end{pmatrix} \begin{pmatrix} \Delta_x(\widehat{U}) \\ \Delta_y(\widehat{U}) \end{pmatrix} \right). \tag{2.2}$$

Equation (2.2) leads directly to the five-point scheme

$$\widehat{U}^{k+1}_{i,j} = \widehat{U}^k_{i,j}(1 - 2(\rho_1 d_{xx} + \rho_2 d_{yy})) + (\widehat{U}^k_{i+1,j} + \widehat{U}^k_{i-1,j})(\rho_1 d_{xx}) + (\widehat{U}^k_{i,j+1} + \widehat{U}^k_{i,j-1})(\rho_2 d_{yy}),$$

where for ease in writing, $\rho_1 = \frac{\Delta t}{(\Delta x)^2}$ and $\rho_2 = \frac{\Delta t}{(\Delta y)^2}$. [3]

A Taylor analysis of this scheme reveals that it has local accuracy $O\left(\Delta t + (\Delta x)^2 + (\Delta y)^2\right)$, which means that the difference between the actual solution and the approximation, or $(U - \widehat{U})$, goes to zero as Δx, Δy, and Δt all go to zero. Further, a von Nuemann analysis shows that the solution is stable as long as $\rho_1 < 0.25$ and $\rho_2 < 0.25$. Thus, the number of time steps significantly restricts the refinement of the diffusion tensor. Since the maximum value in both D and $\overline{D}$ is less than 1.02, it was sufficient to impose the restriction $\rho_1 < 0.245$ and $\rho_2 < 0.245$. [2]

The implementation of the constant initial and boundary conditions into the numerical scheme was straightforward. In order to put the no-flux condition into practice, we referred again to the approximation of the first-order spatial derivative. The condition stated that $\frac{\partial}{\partial y}(U(x,0,t)) = 0$, which translates into $\frac{1}{\Delta y}\left(\widehat{U}^k_{i,0} - \widehat{U}^k_{i,-1}\right) = 0 \Rightarrow \widehat{U}^k_{i,0} = \widehat{U}^k_{i,-1}$ for all i and k. Thus, we merely substituted $\widehat{U}^k_{i,0}$ for any computation requiring $\widehat{U}^k_{i,-1}$.

A computer program was written that computed $\widehat{U}^{k+1}_{i,j}$ for $k = 1, \ldots, n_t$ using three basic loops. The inner loop cycled i from 1 to n_x, while the middle loop cycled j from 1 to n_y. The outer loop ran through all values of k from 1 to n_t. At the beginning of each outer loop, the points along $y = 0$ were reset to the profile temperature, providing the forcing to the system.

2.3 Choosing a Homogenized Value for $D(x, y)$

In order to determine the necessary degree of homogenization, a simulation with actual diffusion coefficients would need to be available for comparison with simulations using averaged diffusion. To save time at this stage, it was decided to run these simulations on

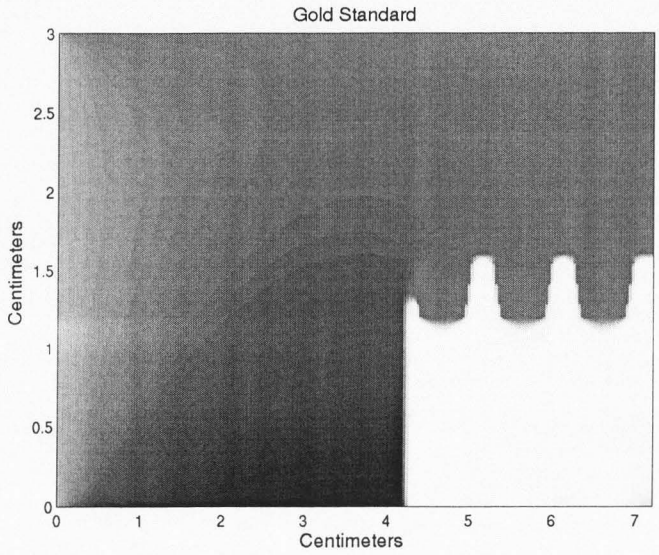

Figure 2.2. Time slice ($t = 23$ seconds) of the standard simulation using actual diffusion values at thirty-two (32) horizontal nodes per well. This simulation is the standard by which the simulations using homogenized diffusion tensors are judged.

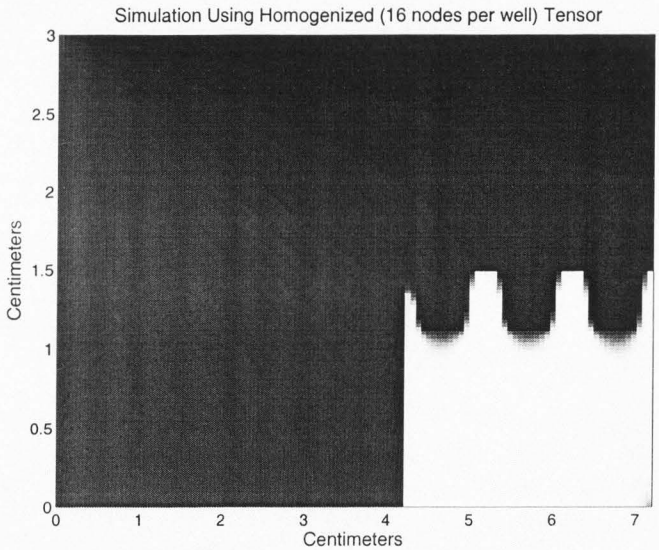

Figure 2.3. Time slice ($t = 23$ seconds) of the simulation using homogenized values at 16 horizontal nodes per well. The structure of the simulation using heterogenous coefficients can readily be seen in this time slice, as expected.

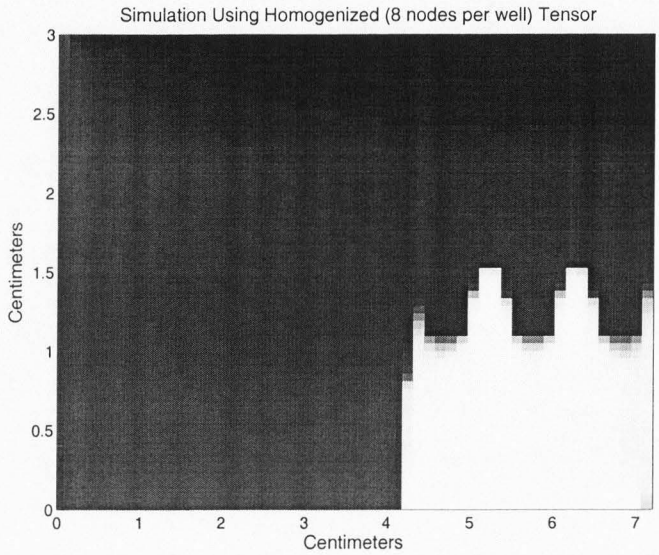

Figure 2.4. Time slice ($t = 23$ seconds) of the simulation using homogenized values at 8 horizontal nodes per well. It was decided from graphical results that this level of homogenization would retain enough of the desired structure, and still decrease the running time of the simulation significantly.

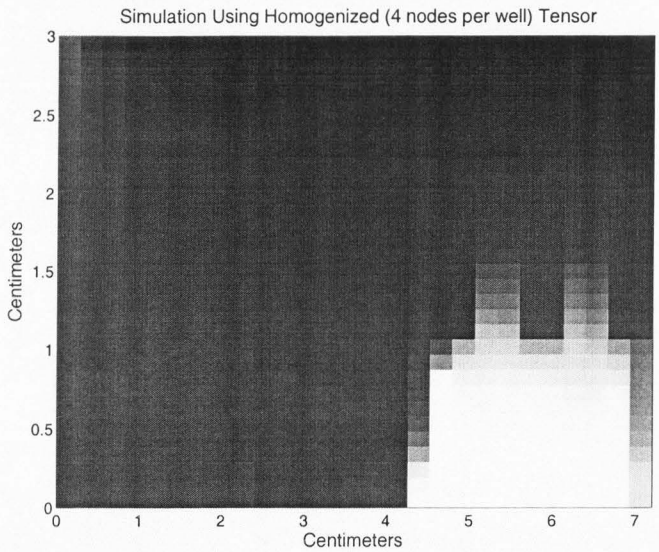

Figure 2.5. Time slice ($t = 23$ seconds) of the simulation using homogenized values at 4 horizontal nodes per well. Initially we had hoped that this level of homogenization would provide enough of the structure inherent in the simulation using heterogenous diffusion, as it would have significantly reduced the running time of simulations. However, the amount of fidelity lost using this level of homogenization was too great.

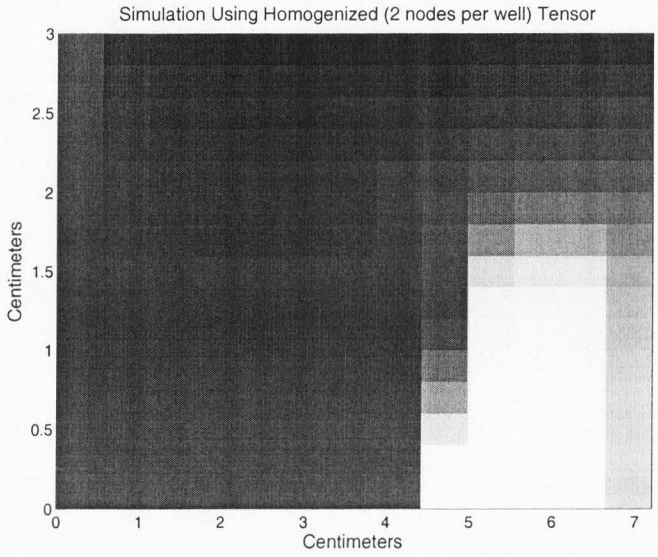

Figure 2.6. Time slice ($t = 23$ seconds) of the simulation using homogenized values at 2 horizontal nodes per well. This level of homogenization doesn't come close to retaining the necessary structure of the standard.

only three wells of the cross-section subject to essentially the same boundary conditions described in Section 2.1. The diffusion tensor of this simulation represented the first 3.4 cm–2 cm of air on the left and 1.4 cm for the three wells–of the complete simulation. On the right side we imposed a no-flux condition, $\frac{\partial}{\partial x}\left(U(3.4, y, t)\right) = 0$, due to the symmetry in the geometry of the problem, in place of the constant boundary condition found in the full scheme.

The standard by which the averaged values were to be measured was a simulation in which each well was made up of 32 horizontal and 256 vertical discrete points. Hereafter, we will describe a specific discretization only in terms of the number of horizontal nodes in one well, and it will be assumed that the number of discrete vertical points per well is four (4) times the number of horizontal points. The homogenization program that was used preserved the aspect ratio of the grid size, and homogenized values of the diffusion tensor were computed on grid sizes of 2×8, 4×16, 8×32, and 16×64. Some graphical results of this experiment are shown in Figures 2.2-2.6. These initial graphical results suggested that a discretization with 8 nodes per well would contain enough of the true structure to provide

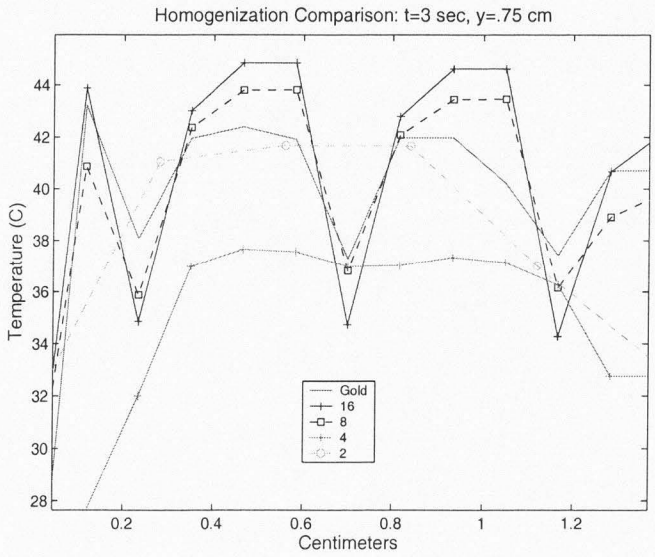

Figure 2.7. Temperatures along the cross-section at a height of .75 cm (the approximate vertical center of the well) after 3 seconds. Notice that as the level of homogenization increases, the profiles seem to be converging to the standard.

accurate results. Further examination of temperature profiles at the center of the well (.75 cm above the circuit) at two different times, shown in Figures 2.7 and 2.8 concur that an average using 8 points per well is sufficient. It is interesting to note that the average using 8 points per well is closer to the standard than the one using twice as many points per well. Using this level of homogenization, the amount of time it took to run one simulation was 30 seconds, compared to roughly 3 minutes using the original heterogenous coefficients.

2.4 The Optimization Process

In order to make the optimizing procedure tractable, we began by assuming that the initial temperature profile came from the family of continuous functions of the form $\phi(x) = a_1 + a_2|x - \alpha|^{a_3}$, where a_1, a_2, a_3 are real numbers and α is the horizontal center of the cross-section (for the section under analysis, $\alpha = 3.65$ cm). Next we assumed that ϕ was a pdf on the interval $[0, 2\alpha]$. The purpose of this assumption was to provide a method of translating a continuous source function into a design of elements on the circuit card. Once the optimal forcing function was found, its distribution function would be computed and then n evenly spaced points from the unit interval would be projected onto the x-axis using

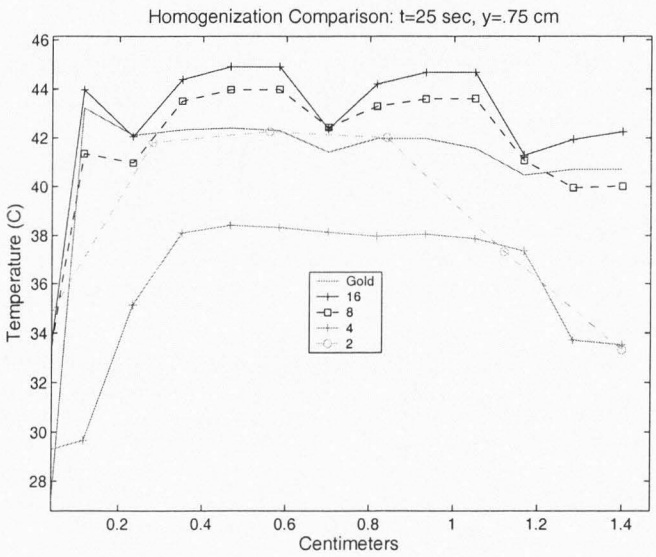

Figure 2.8. Temperatures along the cross-section at a height of .75 cm (the approximate vertical center of the well) after 25 seconds. Interestingly, throughout most of the cross-section the 8-node homogenized simulation actually comes closer to approximating the standard than the 16-node approximation. This observation made the 8-node level even more desirable.

the distribution as functional values, as shown in Figure 2.9. These projected values would be the locations that we would place constant heating elements.

In addition to transforming a continuous profile into a discrete array for the circuit card, the fact that ϕ is a pdf helped reduce the dimension of the parameter space from 3 to 2 since the parameter a_1 is easily determined by the equation

$$\int_0^{2\alpha} (a_1 + a_2|x - \alpha|^{a_3})\, dx = 1,$$

once a_1 and a_2 are fixed. Further, it is the case that $\phi(x) \geq 0$ for all x in the interval $[0, 2\alpha]$ and this stipulation provides the the restriction $a_1 \geq 0$ and $a_1 + a_2\alpha^{a_3} \geq 0$. With this constraint range, a method of measuring the relative effectiveness of the profile for a given choice of a_2 and a_3 was devised.

The model was executed using ϕ as the forcing function along $y = 0$. After the simulation was complete, the mean of the temperatures at the center point of each well was computed at 32 different time intervals, ranging from 0 to 40 seconds. Denote the mean temperature at time step k by $\overline{\tau}_k$, and the temperature in the r^{th} well at time step k by τ_r^k. At each

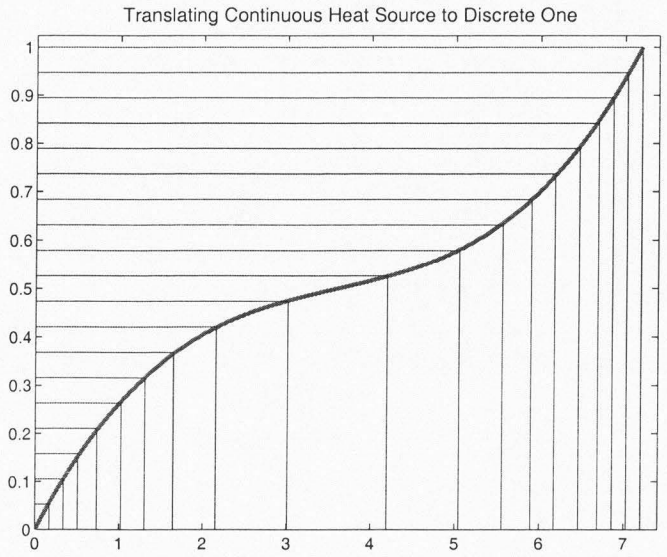

Figure 2.9. Projection process for the forcing function $\phi(x)$ with parameter values $a_1 = 0.0394856\overline{8}$, $a_2 = 0.02301$, $a_3 = 2$. The red curve is the cumulative distribution function (cdf) of $\phi(x)$. The 19 horizontal lines represent the uniform heat output we desire. The intersection of these lines and the cdf are projected onto the x-axis and these projected points represent the locations where heating elements should be placed.

time step k, the temperature at each of these wells was measured against the mean using the Euclidean norm

$$E_k = \sqrt{\sum_{r=1}^{16} (\overline{\tau}_k - t_r^k)^2},$$

and a percentage error norm

$$P_k = \frac{1}{16} \sum_{r=1}^{16} \left(1 - \frac{|\overline{\tau}_k - \tau_r^k|}{\overline{\tau}_k} \right).$$

These norms were then averaged over the 32 time intervals and ϕ was assigned values $\overline{E} = \frac{1}{32} \sum E_k$ and $\overline{P} = \frac{1}{32} \sum P_k$. In addition to these measures, a correlation coefficient, R^2, was computed for the vectors M and T_ϕ, of length $(16 \cdot 32)$ which are defined by

$$M = \left(\overrightarrow{\vartheta}_1, \overrightarrow{\vartheta}_2, \ldots, \overrightarrow{\vartheta}_{32} \right), \quad \overrightarrow{\vartheta}_i = \underbrace{(\overline{\tau}_i, \overline{\tau}_i, \ldots, \overline{\tau}_i)}_{16 \ \overline{\tau}_i}$$

and

$$T_\phi = \left(\tau_1^1, \tau_2^1, \ldots, \tau_{16}^1, \tau_1^2, \tau_2^2, \ldots, \tau_1^{32}, \tau_2^{32}, \ldots, \tau_{16}^{32} \right).$$

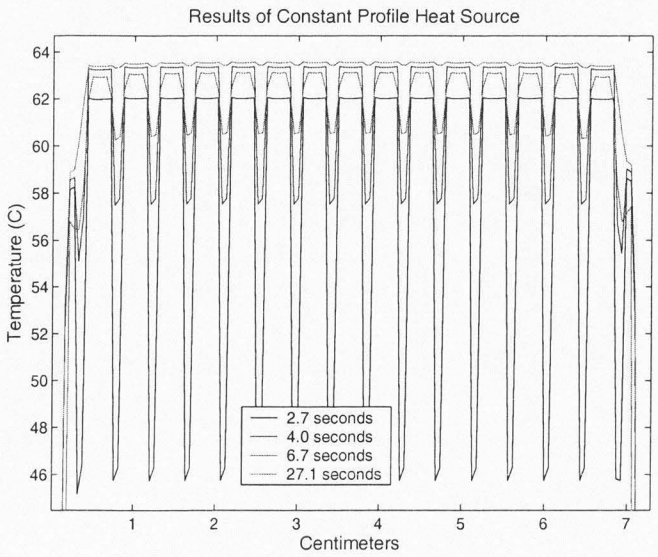

Figure 2.10. Temperature profile of cross-section of well .75 cm above the circuit card using a continuous constant profile as the heat source. Though the temperatures in the end wells are lower, the uniformity among the middle 14 wells caused the constant profile to perform the best under our examination method.

After an initial trial with $a_3 = 2$, it was determined that the $\overline{E}$ measure would most clearly identify an optimal forcing function. Later, upon suggestion, we incorporated the sup norm measure $S_k = max\left(|\overline{\tau}_k - \tau_r^k|\right)$, with $\overline{S} = \frac{1}{32}\sum S_k$ to try to improve results, and found that it is actually preferable to the $\overline{E}$ norm, as noted later on.

The results of the initial attempt at optimization using ϕ and the $\overline{E}$ norm were educational. After checking literally thousands of different initial profiles, the program surprisingly deemed as the temperature-uniformity-optimizing profile a constant function. Figure 2.10 and 2.11 may help explain why this happened. Figure 2.10 shows the results of the simulation with a constant profile. The temperatures in the fourteen middle wells are essentially identical and the plastic edge of the tray appears to have only a slight effect on the end wells. Contrast this with Figure 2.11, in which, the end wells are brought up in temperature, but at a significant cost of variability among the middle wells.

Using the knowledge of the first attempt, a second family of profiles was constructed. These profiles, one of which is depicted in Figure 1.1, are piece-wise continuous functions made up of linear and constant functions and are symmetric around $x = \alpha$. For the same

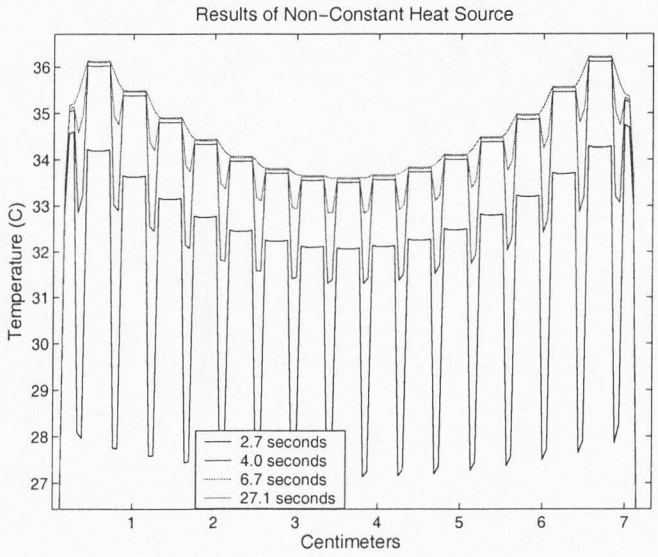

Figure 2.11. Temperature profile of cross-section of well .75 cm above the heat source using as a heat source the function $\phi(x) = a_1 + a_2|x - \alpha|^{a_3}$ with parameters $a_1 = 0.134568$, $a_2 = 0.001$, and $a_3 = 2$. Using this profile as the heating source is not preferable since the cost of bringing up the temperature in the end wells is considerable variation in temperature among the middle wells.

reasons previously explained, we normalized these functions and required them to be density functions on the interval representing the instrument cross section, $[0, 2\alpha]$.

We proceeded as before, computing κ from the integral equation after choosing β and γ values. As both β and γ varied within their constraint range, the $\overline{E}$ norm was once again used to gauge the value of each function as a uniformity optimizing profile. The results of this search, shown in Figure 2.12 suggested that the optimal profile of the family is the one having parameter values $\beta = 0.4774$, $\gamma = 0.0055$, and $\kappa = 0.1385$.

Though this result was arguably more informative than the previous one, the optimal profile (shown in Figure 2.16 multiplied by 70α–see Appendix B for an explanation of this constant), turned out to produce a distribution function that was nearly linear. This was not surprising since the bulk of the profile is constant, and the slope of the lines on each end is minimal.

As previously mentioned, we instituted another method of measuring forcing functions based on the sup norm, $\overline{S}$, defined above and tested both forcing designs using this mea-

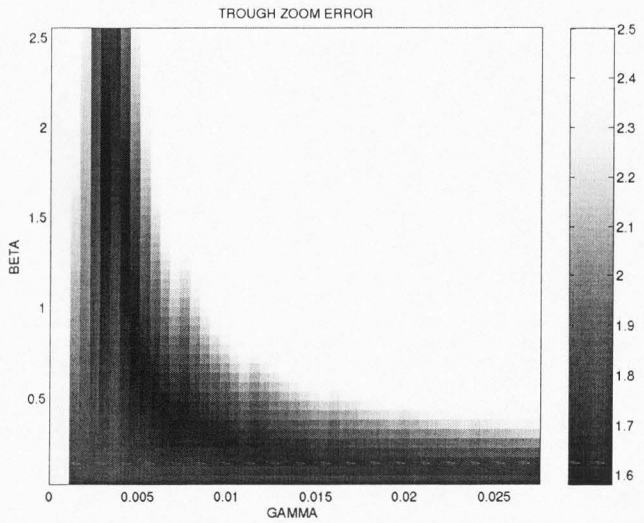

Figure 2.12. The results of the trough function search using the $\overline{E}$ norm. The colors represent the value $\overline{E}$ that was assigned to each function for corresponding choices of β and α. The optimal design according to these experiments is the one with parameters $\beta = 0.4774$, $\gamma = 0.0055$, and $\kappa = 0.1385$.

surement. Figures 2.14 -2.18 summarize these experiments. It is noteworthy that this new measurement did not select a constant from the ϕ functions as the optimal heat source. This is most likely due to the fact that discrepancies in temperature at the edge wells are accentuated when using the $\overline{S}$ norm. Due to this property of the $\overline{S}$ measure, it is, in most circumstances, preferable to the $\overline{E}$ norm.

The optimal trough function chosen using the $\overline{S}$ norm were very close to that chosen under the $\overline{E}$ norm. For the $\overline{S}$ norm, the optimal function parameters are $\beta = 0.4744$, $\gamma = 0.0085$, and $\kappa = 0.1383$. Due to this fact and the comments in the previous paragraph, it seems that $\overline{S}$ is a more useful measure.

2.5 Conclusion

Due to the low thermal diffusion coefficient of the plastic (around 0.0025 $cm \cdot sec^{-2}$) that surrounds the Idaho Technology *LightTyper* instrument, it was the belief of the author that significant adjustments needed to be made to the design of the circuit card to account for this fact. As a consequence, a number of different forcing functions which had significantly

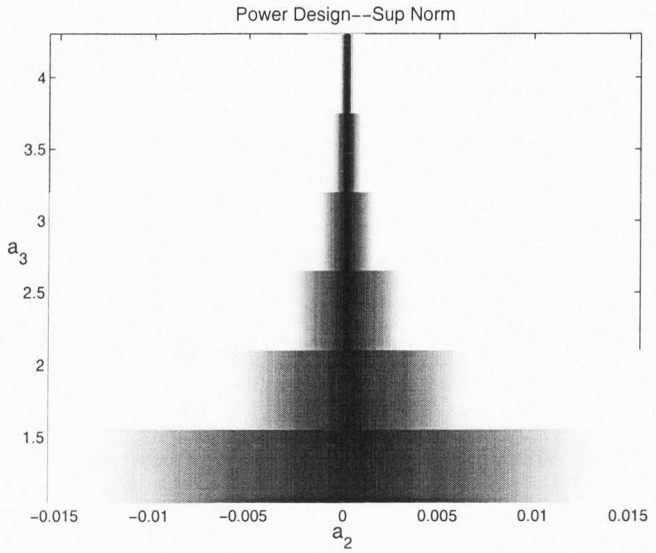

Figure 2.13. Results of the search for an optimal profile among heat sources of the form $\phi(x) = a_1 + a_2|x - \alpha|^{a_3}$ using the sup norm. The optimal source function from this family has parameters $a_1 = 0.138024\overline{8}$, $a_2 = 0.0002$ and $a_3 = 2$. This result infers that the sup norm is more informative than the Euclidean norm as the latter selected a constant forcing function as optimal under an identical search.

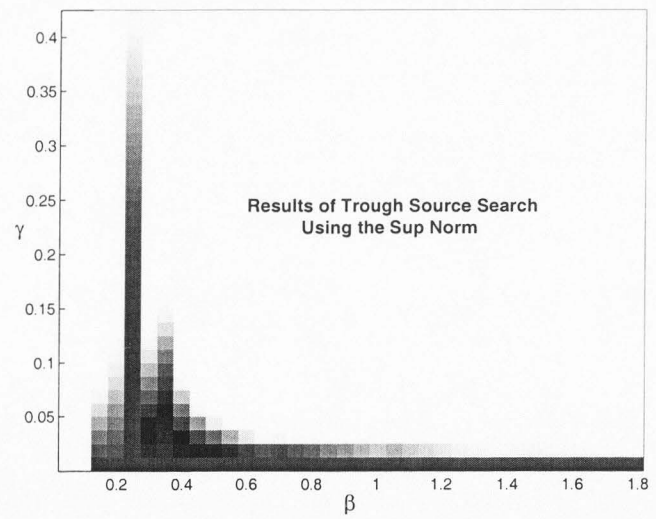

Figure 2.14. Results of the search for an optimal trough function using the sup norm measure $\overline{E}$. The optimal profile in this experiment was extremely close to the optimal profile found using the Euclidean norm $\overline{E}$. The optimal parameters from this search were $\beta = 0.4744$, $\gamma = 0.0085$, and $\kappa = 0.1383$.

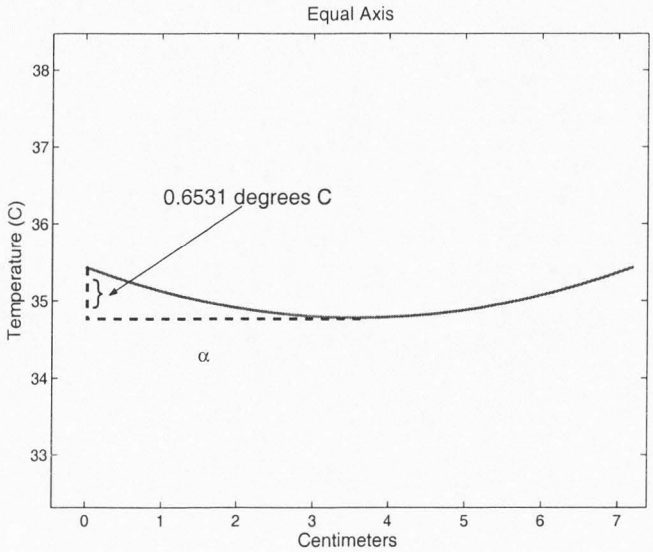

Figure 2.15. Plot of the source function $\phi(x) = a_1 + a_2|x - \alpha|^{a_3}$ with values $a_1 = 0.138024\overline{8}$, $a_2 = 0.0002$ and $a_3 = 2$. This function was chosen as the source that effectively maintains uniformity of temperature within wells using the sup norm. The graphic confirms that in order to adjust for the plastic around the end wells only a small increase in temperature $(0.6531°C)$ is required at the edges.

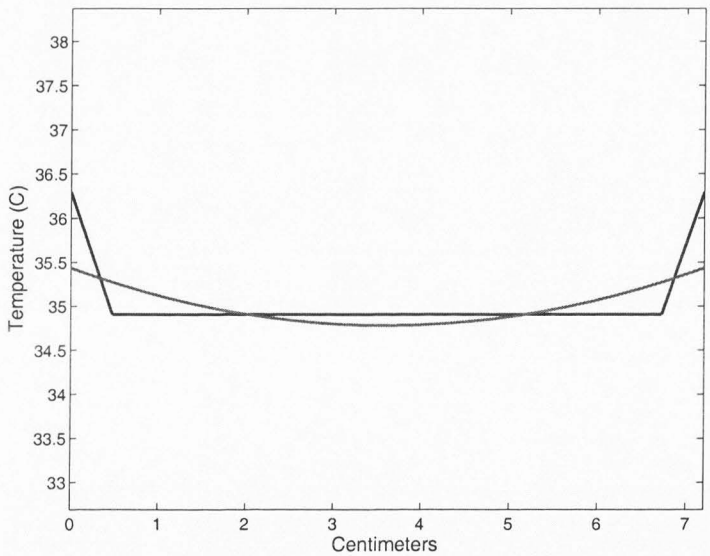

Figure 2.16. Plot showing the optimal heating sources from each family of designs. The differences in the basic structure of each design is quite apparent, yet each produced the best measure using the $\overline{S}$ norm. The question that follows naturally from this point is, "Which of these two source functions performs better under more extensive analysis when compared head to head?"

higher values at each end of the instrument interval $[0, 2\alpha]$ were tested and measured for their ability to maintain consistency of temperature within the wells of the machine. However, a major conclusion that the results of this project has identified is that the edge effects do not play as significant a role as was previously thought.

Having said that, we also declare that a constant profile is inadequate. As Figure 2.10 describes, a constant forcing function is not optimal, as it leaves the end wells considerably lower than their counterparts in the middle. Thus, in the two-dimensional cross-section, it is the case that a significant portion of the optimal forcing function must be constant with some adjustment, smaller than previously thought, on the edges.

The ideas, principles, and foundations laid forth in this paper could easily be adapted and used to identify more specifics of an optimal forcing function and circuit card design for the two-dimensional case. Further, in the author's estimation, having a model that simulates heat flow through all three spatial dimensions of the machine is critical in finding a clear description of the circuit card design that will optimize the uniformity of heat within the wells.

REFERENCES

[1] M. Holmes, *Introduction to Perturbation Methods*, Springer-Verlag, New York, 1995.

[2] A. Mitchell and D. Griffiths, *The Finite Difference Method in Partial Differential Equations*, John Wiley and Sons, New York - Toronto, 1987.

[3] G. Sewell, *The Numerical Solution of Ordinary and Partial Differential Equations*, Harcourt Brace Jovanovich, Boston, 1988.

[4] C. Wittwer, M. Herrmann, A. Moss, and R. Rasmussen, *Continuous fluorescence monitoring of rapid cycle dna amplification.*, BioTechniques, 22 (1997), pp. 130–138.

APPENDICES

APPENDIX A

BRIEF HOMOGENIZATION THEORY

Homogenization is an averaging technique used to simplify problems with inherent variations over disproportionate length scales. Typically, an average is sought to smooth out a complex substructure, and the role of homogenization answers the question, 'Which average is best?'. One feature of the homogenization process is that it is very problem dependent; that is, there is not one general algorithm that one may apply to a general problem. The details and specifics of the substructure under critique help guide one through the homogenization process. This being the case, we will present the basics of a simple one-dimensional example to help elucidate the major components of the technique. Consider the problem found in [1] of obtaining the solution to the following ordinary differential equation:

$$\frac{d}{dx}\left(D(x)\frac{d}{dx}u(x)\right) = f(x), \qquad 0 < x < 1, \tag{A.1}$$

where D is some sort of diffusion whose graph is shown in Figure A.1. Notice from that figure the two levels of structure found in D : on the large scale, $x \in [0,1]$, D is increasing in almost a linear fashion, and on the small scale ($x \in [(n-1)(0.0625), n(0.0625)]$, $n = 1, 2, \ldots, 16$), D is periodic–with relatively large amplitude–in nature.

The first step in the homogenization process is to choose a value, ε, which depends on the substructure, as shown in Figure A.2. Next, the micro-scale, or fast scale, variable ξ is defined as follows $\xi = \frac{x}{\varepsilon}$. Note that as x ranges from 0 to ε, ξ ranges from 0 to 1. We next assume that u, D, and f and are all functions of both x and ξ, and perform a perturbation analysis of the differential equation (A.1) in terms of ε. That is, we assume that the functions u and f may be approximated by

$$u(x,\xi) = u_0(x,\xi) + \varepsilon u_1(x,\xi) + \varepsilon^2 u_2(x,\xi) + \cdots,$$

and

$$f(x,\xi) = f_0(x,\xi) + \varepsilon f_1(x,\xi) + \varepsilon^2 f_2(x,\xi) + \cdots.$$

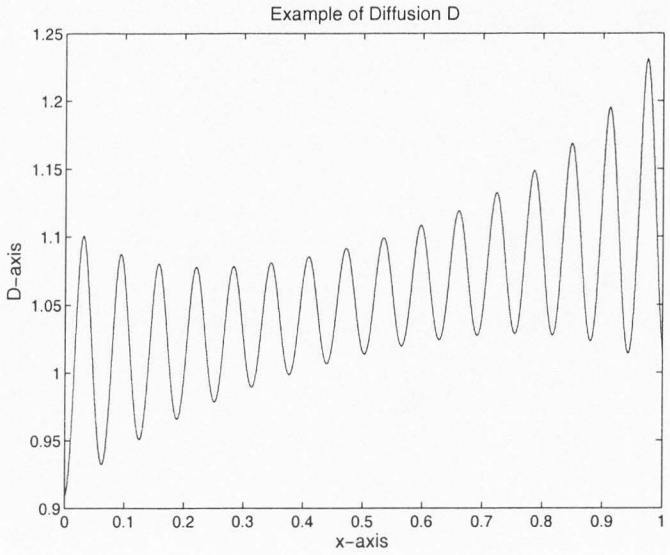

Figure A .1. Diffusion function $D(x) = (1 + \alpha x + \beta g(x) cos(\xi))^{-1}$, with parameters $\xi = \frac{x}{\varepsilon}$, $g(x) = e^{4x(x-1)}$, $\alpha = -0.1$, $\beta = 0.1$, and $\varepsilon = 0.01$. Notice the periodic substructure inherent in the function D. The process of homogenization attempts to smooth out that complex substructure, which makes equation A.1 hard to solve, even numerically.

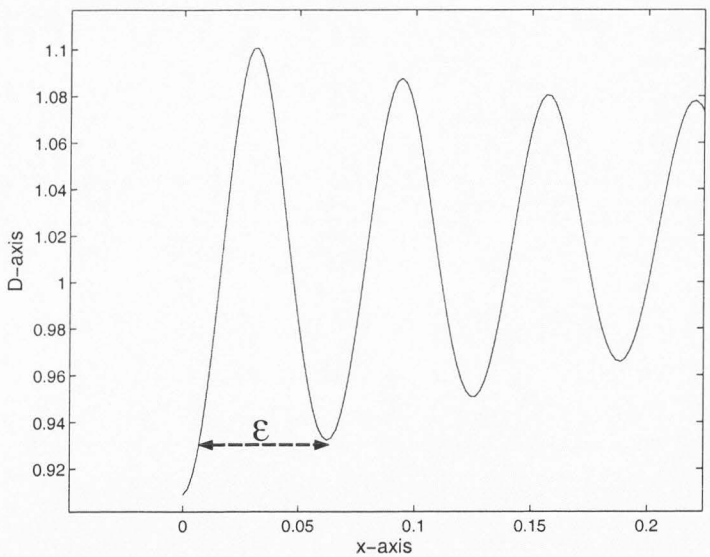

Figure A .2. A close-up of the diffusion function D. A key to obtaining a successful homogenization average is choosing the variable ε, which depends on the substructure of the problem. Here ε is the length of one period of the substructure of D.

Following this we substitute these approximations into equation (A.1), noting that, by definition of ξ, $\frac{d}{dx} \rightarrow \frac{d}{dx} + \frac{1}{\varepsilon}\frac{d}{d\xi}$. Terms are grouped according to order of ε and a new set of differential equations is obtained. The next crucial step, which again depends on the problem, is to compute an average for D (usually an integral average) which helps to balance out this new set of differential equations. An effectively chosen average $\overline{D}$ will now be a function of only the macro-scale x, as will be the functions u_0 and f_0. Thus, equation (A.1) has been replaced by the approximation

(A .2)
$$\frac{d}{dx}\left(\overline{D}(x)\frac{d}{dx}u_0(x)\right) = f_0(x),$$

and as desired, no function in equation (A.2) depends on the micro-scale variable ξ . In a sense we've smoothed out the complexities in the substructure and are now able to solve the latter equation quite easily, whereas our original problem would be challenging to solve, even numerically. [1]

APPENDIX B

SCALING THE FORCING FUNCTION

We now give mathematical reasoning for scaling the forcing functions in order to bring their heat up sufficiently to obtain a proper simulation.

Suppose there exists an equation U that satisfies the equations

$$\frac{\partial U}{\partial t} = \nabla \cdot (D \nabla U) \tag{B .1}$$

and

$$U(x, 0, t) = g(x) = \alpha f_1(x) + \beta f_2(x) \tag{B .2}$$

as well as appropriate initial and boundary conditions all of the form

$$R_i = \alpha r_i + \beta s_i.$$

Further assume that there exist functions u_1 and u_2 that satisfy

$$\frac{\partial u_1}{\partial t} = \nabla \cdot (D \nabla u_1), \qquad u_1(x, 0, t) = f_1(x) \tag{B .3}$$

$$\frac{\partial u_2}{\partial t} = \nabla \cdot (D \nabla u_2), \qquad u_2(x, 0, t) = f_2(x), \tag{B .4}$$

as well as the initial and boundary conditions r_i and s_i, respectively. If these conditions are satisfied, then we claim $U = \alpha u_1 + \beta u_2$.

Since the $\frac{\partial}{\partial t}$ operator is linear it is the case that

$$\frac{\partial}{\partial t}(\alpha u_1 + \beta u_2) = \alpha \frac{\partial u_1}{\partial t} + \beta \frac{\partial u_2}{\partial t}.$$

Similarly since the ∇ operator is linear we have

$$\nabla \cdot (D[\nabla(\alpha u_1 + \beta u_2)]) \quad = \quad \nabla \cdot (D[\alpha \nabla u_1 + \beta \nabla u_2])$$

$$
\begin{aligned}
&= \nabla \cdot (\alpha D \nabla u_1 + \beta D \nabla u_2) \\
&= \alpha \nabla \cdot (D \nabla u_1) + \beta \nabla \cdot (D \nabla u_2).
\end{aligned}
$$

Then by equations (B.2) and (B.3) we see that

$$
\begin{aligned}
&\frac{\partial}{\partial t}(\alpha u_1 + \beta u_2) - \nabla \cdot (D[\nabla(\alpha u_1 + \beta u_2)]) = \\
&\alpha \frac{\partial u_1}{\partial t} + \beta \frac{\partial u_2}{\partial t} - \alpha \nabla \cdot (D \nabla u_1) + \beta \nabla \cdot (D \nabla u_2) = \\
&\alpha \left(\frac{\partial u_1}{\partial t} - \nabla \cdot (D \nabla u_1) \right) + \beta \left(\frac{\partial u_2}{\partial t} - \nabla \cdot (D \nabla u_2) \right) = \alpha \cdot 0 + \beta \cdot 0 = 0,
\end{aligned}
$$

and $\alpha u_1 + \beta u_2$ satisfies equation (B.1).

More importantly, we have

$$
\alpha u_1(x, 0, t) + \beta u_2(x, 0, t) = \alpha f_1(x) + \beta f_2(x) = g(x),
$$

and $\alpha u_1 + \beta u_2$ satisfy equation (B.2) also.

Since $\alpha u_1 + \beta u_2$ satisfy the exact initial and boundary conditions that U does, by the uniqueness theorem, it must be the case that $U = \alpha u_1 + \beta u_2$, and scaling a heating source function is justified.

It was decided, due to a study of the temperatures needed to achieve success throughout the polymerase chain reaction, that the heat of each of the discrete elements would remain at a constant temperature of 70°. We wanted the energy of the continuous heating source to have the same energy as the actual machine and therefore used the following argument to arrive at the constant 70α. Let E represent the total energy of the forcing function. Regardless of what function $\phi(x)$ we use as the heat source, it must be the case that

$$
70 = E = c \left(\int_0^{2\alpha} \phi(x) dx \right),
$$

where c is an unknown constant. Since ϕ is a pdf, it must be the case that $c = 70$. Thus, over the entire interval, we desire the energy integral of the forcing function to be 70α.